ELSEVIER

Materials Science and Engineering B66 (1999) 189–193

MATERIALS SCIENCE & ENGINEERING B

www.elsevier.com/locate/mseb

Failure analysis of heavily proton irradiated p^+-n InGaP solar cells by EBIC and cathodoluminescence

M.J. Romero [a,*], R.J. Walters [b], D. Araújo [a], R. García [a]

[a] Dept. de Ciencia de los Materiales e I.M. y Q.I., Facultad de Ciencias, Universidad de Cádiz, Apdo. 40, E-11510, Puerto Real, Cádiz, Spain
[b] Naval Research Laboratory, Code 6615, 4555 Overlook Ave., S.W., Washington, DC 20375, USA

Abstract

In this paper the effects of heavy proton irradiation on single-junction (SJ) p^+-n InGaP solar cells are investigated by means of electron-beam-induced-current (EBIC) and cathodoluminescence (CL). A hole diffusion length reduction from 0.3 to 0.02 μm after 1×10^{14} protons/cm^2 irradiation is estimated from EBIC measurements. Such degradation is attributed mainly to IE3 point defects as evidenced by the temperature dependence of the CL intensity. The electronic activity of such defects is shown to be reduced after thermal treatment. Indeed an enhancement of the light emission is observed after electron bombardment only on InGaP while no recovery is observed on the GaAs substrate. Such results illustrate the potential of EBIC/CL in device failure analysis as they are non-destructive techniques. © 1999 Elsevier Science S.A. All rights reserved.

Keywords: Heavy proton irradiation; Electron-beam-induced-current (EBIC); Cathodoluminescence (CL); InGaP solar cells; Device failure

1. Introduction

The volume of data transfer required by the new communication systems makes necessary satellite networks in orbits in or near the proton radiation belts, which extend from approximately 2000–10 000 km (MEO: Medium-Earth Orbit) [1]. Such satellites suffer high cosmic irradiation. The space photovoltaic devices of the latter satellites require solar cells delivering high power densities with low degradation under cosmic particle bombardment. Among the different materials tested for spatial applications, $In_{0.5}Ga_{0.5}P$ (hereafter, $InGaP_2$) has been demonstrated to be relatively resistant to particle irradiation and to deliver the best EOL (end-of-life: 1×10^{15} cm^{-2} 1 MeV electron fluence) power density. Indeed values of 25 mW/cm^2 (1 sun, AMO) are demonstrated for InGaP solar cells while GaAs/Ge or InP/Si devices lie below 18 mW/cm^2 [2–4]. Moreover, due to its wide bandgap (1.9 eV), it is very suitable as a top cell in dual-junction (DJ) technology [5]. The latter uses the multiple junction technique, each one with a different material bandgap, to enhance the sensitivity to solar spectral radiation. In this contribution, we investigate the effects of 3 MeV proton irradiation at fluences of 1×10^{14} protons/cm^2 on single-junction (SJ) p^+-n $InGaP_2$ solar cells. The electron-beam-induced-current (EBIC) and cathodoluminescence (CL) techniques of the scanning electron microscope (SEM) are used to study the optoelectronic and microelectronic device failure in terms of the spatial distribution of diffusion length and radiative and non-radiative recombination centers.

2. Experimental details

The p^+-n SJ InGaP cells were grown by OMVPE on n^+ GaAs substrates at The Research Triangle Institute. The solar cell heterostructure is shown in Table 1. The cell total area is 0.254 cm^2 with an active area of 0.16 cm^2. The 3 MeV proton irradiations were performed at Naval Surface Warfare Center Pelletron facility in White Oak, MD. The dosimetry accuracy is estimated to be approximately 10%.

For the EBIC measurements, a cell was mounted on an adapted holder of a Jeol-JSM820 SEM in the planar configuration, with the incident electron beam perpendicular to the junction. The EBIC current (I_{cc}) was measured using a head pre-amplifier followed by a low

* Corresponding author.
E-mail address: manueljesus.romero@uca.es (M.J. Romero)

0921-5107/99/$ - see front matter © 1999 Elsevier Science S.A. All rights reserved.
PII: S0921-5107(99)00096-3

Table 1
SJ p^+-n InGaP solar cell structure

Material	Function	Thickness (μm)	Carrier density (cm^{-3})
p^+ GaAs	Cap	0.2	1×10^{19}
p AlInP	Window	0.025	8×10^{17}
p^+ InGaP		0.05	4×10^{18}
p^+ InGaP	Emitter	0.2	2×10^{18}
n InGaP	Base	1	$\sim1\times10^{16}$
n^+ InGaP	Back-surface field (BSF)	0.02	1×10^{18}
n^+ GaAs	Buffer	0.4	2×10^{18}
n^+ GaAs	Substrate	250	2×10^{18}

input impedance amplifier (Matelect-5A). The electron beam current (I_b) was measured by a Faraday cup. Both are collected at different electron beam energies between 1 and 30 keV. The electron beam energy dependence of the EBIC gain (I_{cc}/I_b) allows an estimate of the in-depth distribution of the minority carrier diffusion length.

The CL experiments were carried out on a freshly cleaved {110} face perpendicular to the p^+-n InGaP junction plane. CL profiles and spectra are recorded in the excitation range between 5 and 30 keV of electron beam energy. A semi-parabolic mirror was attached to an optic guide yielding high efficiency collection of the luminescence. For IR detection a Ge cryo-detector is used (North Coast EO-817L). A cryogenic CCD (Photometrics SDS9000) is attached to an Oriel 77400 Spectrograph/Monochromator for spectroscopic mode of the cathodoluminescence. The CTI-Cryogenics 22C/350C He closed-circuit cryostat attached to an anti-vibration system is used in low temperature (LT) CL experiments. The instrumentation control and data acquisition are computer controlled.

3. Electron-beam-induced-current analysis

Fig. 1 shows the electron beam energy dependence of the EBIC gain for the unirradiated and heavily-proton irradiated SJ p^+-n InGaP cells. For quantitative analysis of the EBIC gain, our approach consisted of first estimating the extent of electron–hole pair (e–h) generation by a Monte Carlo procedure [6]. Second, the Poisson and the e–h current density continuity equations are resolved by applying a self-consistent iterative finite difference method. For the unirradiated (pre-rad) cell, the minority carrier diffusion length at base is estimated to be 0.30 ± 0.01 μm. The emitter acts as a perfect collector of electron beam induced e–h and we estimate a lower limit to the electron diffusion length of 1.5 μm.

The EBIC data for the cell irradiated with 3 MeV

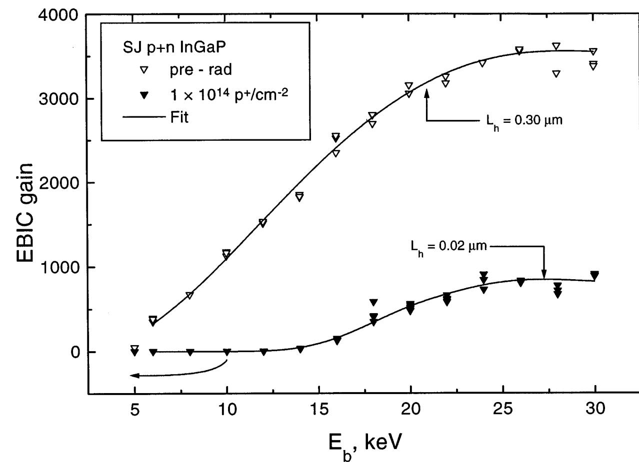

Fig. 1. Experimental and closest-fit electron beam energy dependencies of the EBIC gain for both unirradiated and heavily-proton irradiated SJ p^+-n InGaP solar cells.

protons (1×10^{14} p^+/cm^2) are shown on Fig. 1. The minority carrier diffusion length is estimated to be 0.02 ± 0.01 μm in the cell base. However, the EBIC gain at electron beam energies below 10 keV shifts negative. These data cannot be explained by only a reduction in diffusion length. This suggests a change in the e–h collection mechanism close to the junction. One possibility is that heavy-proton irradiation results in some carrier removal and compensation effects in the p^+ emitter, which are more pronounced at the top of the cell (approximately 75–100 nm in depth). In other words, the result is that the total structure would be p^--p-n and negative EBIC currents are possible when injection carriers only are close to the surface, i.e. at low e-beam voltages. In this case, a non uniform defect distribution would be expected to be induced by proton irradiation.

4. Cathodoluminescence: radiation-resistant and annihilation properties of InGaP

The CL measurements were made on a freshly cleaved {110} face perpendicular to the epilayers and performed between 70 and 300 K. The CL spectra at $T=70$ K from the SJ p^+-n InGaP solar cells are shown in Fig. 2. The CL spectra were recorded at $E_b=20$ keV and $I_b=1.5$ nA with a magnification of 20 000 centered in the p^+-n InGaP junction, in the 1.4–2.0 eV interval. Three peaks are observed: the first at 1.45 eV is attributed to free-to-bound (e, Si^0) transitions, the others correspond to the e–h band-to-band transitions related to GaAs (1.5 eV at $T=0$ K) and $InGaP_2$ (2.0 eV [7] at $T=0$ K, $InGaP_2$). We analyse in the following the relative and absolute CL intensities of the GaAs and InGaP related peaks versus the proton irradiation and the thermal anneal recovering.

First, we observe an impressive decrease of the luminescence after heavy irradiation. The relative GaAs with respect to InGaP peak intensity is 1.5 before the irradiation and falls to 0.6 after the 1×10^{14} protons/cm^2 irradiation at 3 MeV. Even though, the total panchromatic CL falls to a factor of 300 after irradiation. We conclude that the defects induced in the InGaP seem to have a lower electronic activity (higher carrier recombination lifetime) than those induced in the GaAs. The second feature is the ability of each material to recover part of their properties after thermal annealing. This point is of prime importance as the space solar cells work at high temperature and suffer then from continuous irradiation damage and thermal annealing. Fig. 2 (bottom) shows the CL spectrum of the entire region of the inset taken after high-injection with the electron beam ($E_b = 20$ keV and $I_b = 10$ nA for 1 h) in the center of the spectrally analysed region (localised on the p$^+$-n junction). This means that the spectrum has contributions of annealed and non-annealed material. The InGaP CL intensity of the whole region duplicate after annealing. The injection time dependence of the InGaP CL intensity in the center of the white point (e-beam injection coordinate) is shown in Fig. 3. The relative InGaP peak intensity increases by a factor of 8.5 after e-beam bombardment whereas the GaAs emission remains constant during an identical experiment on the GaAs material.

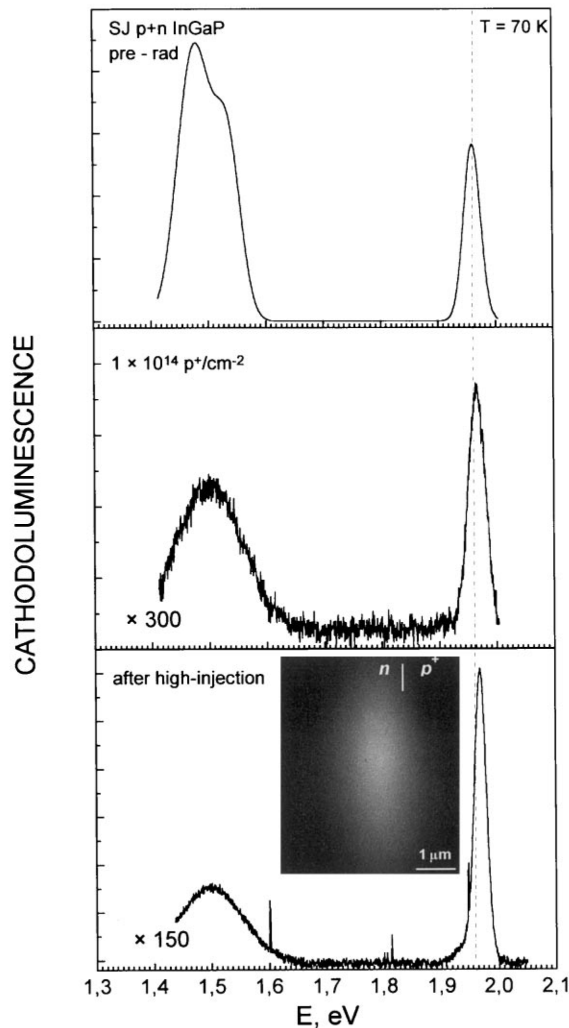

Fig. 2. CL spectra (from top to bottom) of the SJ p$^+$-n InGaP solar cells prior to proton irradiation, after high-energy proton irradiation and after high injection in the p$^+$-n InGaP junction by electron beam excitation ($E_b = 20$ keV and $I_b = 10$ nA for 1 h) of the heavily-proton irradiated SJ p$^+$-n InGaP cell. The radiation-induced shift to minor wavelength of the InGaP-related luminescence is clearly seen by the dash–dot line. The CL micrograph (inset) recorded after high injection with e-beam shows the spatial distribution of the luminescence after recovery.

From the contribution of the InGaP and GaAs related-luminescences to the total CL intensity, the degradation of GaAs seems to be higher than InGaP. The superior defect annihilation properties, and consequently radiation-resistant properties, of InGaP over GaAs are clearly seen in the lower spectrum of Fig. 2 taken after high e–h injection with the electron beam localised on the p$^+$-n InGaP junction of the heavily-proton irradiated cell. After injection annealing, the InGaP luminescence increases whereas the e–h band-to-band emission from GaAs remains constant.

The other experimental feature of the CL spectra is the shift to shorter wavelength (approximately 10 meV) of the InGaP luminescence after irradiation. We attribute it to a radiation-induced-transition from the initial partially ordered ternary alloy to disordered InGaP. It is well known that InGaP has a tendency to order the cations on the group III sublattice producing alternate In- and Ga-rich {111} planes. Ordering is predicted [8] and experimentally observed to result in a decrease in the e–h band-to-band transition energy. The ordering is a kinetic phenomenon that is confirmed experimentally to depend on the misorientation of the substrate [9] and the growth parameters such as the growth temperature [10], V/III ratio [10,11] and growth rate [12]. The SJ p$^+$-n InGaP solar cells were grown by OMVPE on (001) GaAs substrates with a misorientation of 2° in the ⟨110⟩ direction. The growth temperature was 923 K, the V/III ratio 80 and the growth rate 0.08 μm/min. From earlier research [13] these growth parameters and substrate misorientation leads to partially ordered InGaP.

5. Temperature dependence of the cathodoluminescence: defect characterisation

In the previous section, we noted that irradiation induced a lowering of the optoelectronic properties of the material. GaAs regions are shown to degrade more strongly than InGaP ones and the latter recover their properties better after thermal annealing. However, at

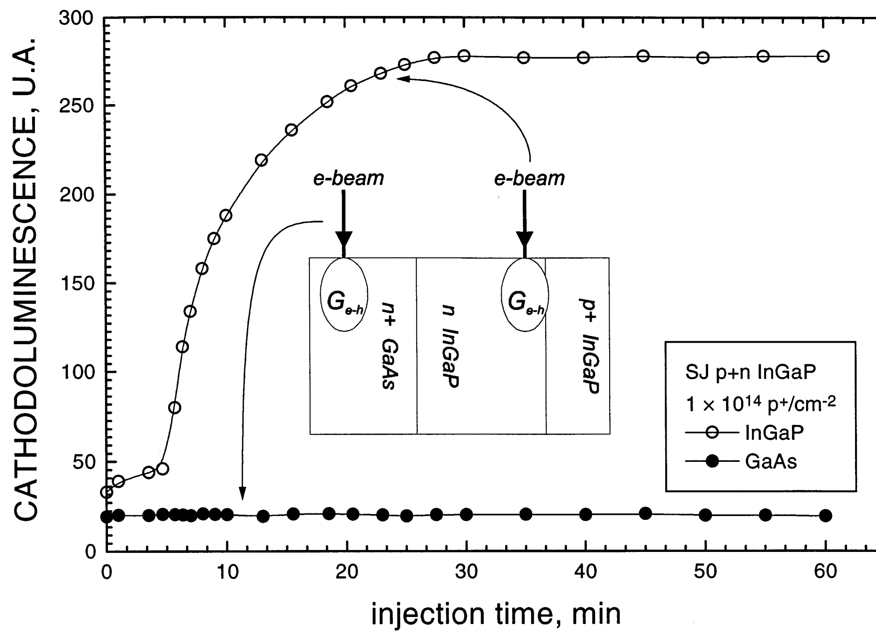

Fig. 3. Injection time dependence of the CL intensity showing the recovery of the InGaP luminescence induced by e-beam bombardment whereas no recovery is observed in GaAs. The geometry of the experiments is displayed in the inset.

this stage of the study, we do not know the nature of the radiation-induced defects. Therefore, we attempt here to determine the binding energy of the states related to these. Indeed, as the radiative recombination has to compete with non-radiative recombinations related to the defect states, the temperature dependence of the CL intensity must follow an Arrhenius behaviour. Then knowing the binding energy, the character of the defect can be determined.

Fig. 4 displays the temperature dependence of the InGaP band-to-band CL intensity of the proton irradiated SJ p^{+}-n InGaP solar cell. It clearly exhibits different intervals that obey an Arrhenius dependence. This behaviour corresponds to different thermally activated non-radiative recombination mechanisms. It will be analysed from the emission efficiency η, that is described by

$$\eta = \left[1 + \kappa^{\alpha}\exp\left(-\frac{E^{\alpha}}{k_{B}T}\right) + \kappa^{\beta}\exp\left(-\frac{E^{\beta}}{k_{B}T}\right)\right]^{-1} \quad (1)$$

where κ is the ratio of radiative to non-radiative recombination lifetimes for each non-radiative recombination mechanism (labelled α and β) at $T = 300$ K and E^{α} and E^{β} are its thermal activation energies. The fit in Fig. 4 results from applying Eq. (1) to the experimental CL data. The fitting parameters were $E^{\alpha} = 1.25$ eV, $E^{\beta} \sim 0.2$ eV, $\kappa^{\alpha} \sim 10^{15}$ and $\kappa^{\beta} \sim 10^{5}$. The α recombination center is assumed to be the previously reported IE3 electron trap [14]. Moreover, Walters et al. [15] also reported IE3 in proton-irradiated InGaP. Measurements at lower temperature would be necessary to increase the accuracy in estimating the energy level of β.

6. Conclusions

We studied the proton irradiation effect on InGaP/GaAs p^{+}-n solar cells using EBIC/CL measurements. A reduction of the diffusion length, probably due to the electronic activity of the radiation-induced defect IE3, is evidenced after proton irradiation. Indeed, the temperature dependence of the CL allows determination of the radiation-induced defect energy levels. The activity of such defects is shown to be reduced after high injection with the electron beam. Such recovery is not observed on GaAs which indicates its lower capacity for spatial applications. The EBIC/CL techniques are

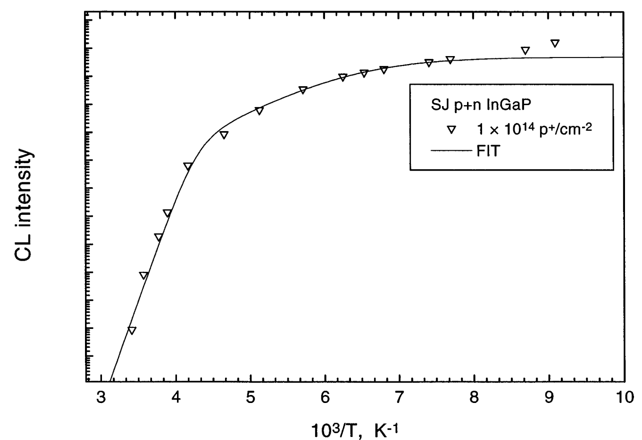

Fig. 4. Arrhenius plot of the temperature dependence of the InGaP band-to-band luminescence intensity in the proton irradiated solar cell. The fit is a result of applying Eq. (1). The level of excitation was $E_{b} = 20$ keV and $I_{b} = 1$ nA.

shown then to be very attractive, as non-destructive techniques, for failure characterisation.

Acknowledgements

This work was supported by the CICYT (Comisión Interministerial de Ciencia y Tecnología) under MAT98-0823-CO3-02 and by the Junta de Andalucía through group TEP-0120. This work was also supported, in part, by the US Office of Naval Research.

References

[1] M. Meyer, R.A. Metzger, Compound Semiconductor 2 (6) (1996) 22.
[2] K.A. Bertness, S.R. Kurtz, D.J. Friedman, A.E. Kibbler, C. Kramer, J.M. Olson, Appl. Phys. Lett. 65 (8) (1994) 989.
[3] J.M. Olson, D.J. Friedman, Compound Semiconductor 2 (6) (1996) 27.
[4] M. Yamaguchi, T. Okuda, S.J. Taylor, T. Takamoto, E. Ikeda, H. Kurita, Appl. Phys. Lett. 70 (12) (1997) 1566.
[5] R.J. Walters, M.A. Xapsos, G.P. Summers, H.L. Cotal, S.R. Messenger, in: 26th IEEE Photovoltaic Specialist Conference, Anaheim, CA, September 1997.
[6] M.J. Romero, D. Araújo, R. García, Appl. Phys. Lett., submitted.
[7] Y. Ishitani, S. Minagawa, T. Tanaka, J. Appl. Phys. 75 (10) (1994) 5326.
[8] R.B. Capaz, B. Koiller, Phys. Rev. B47 (7) (1993) 4044.
[9] H. Murata, I.H. Ho, Y. Hosokawa, G.B. Stringfellow, Appl. Phys. Lett. 68 (16) (1996) 2237.
[10] A. Gomyo, K. Kobayashi, S. Kawata, I. Hino, T. Suzuki, J. Cryst. Growth 77 (1986) 367.
[11] Y.S. Chun, H. Murata, G.B. Stringfellow, J.B. Mullin, J. Cryst. Growth 170 (1-4) (1997) 263.
[12] Y.S. Chu, S.H. Lee, I.H. Ho, G.B. Stringfellow, J. Cryst. Growth 174 (1-4) (1997) 585.
[13] L.C. Su, I.H. Ho, G.B. Stringfellow, J. Appl. Phys. 76 (6) (1994) 3520.
[14] M.A. Zaidim, M. Zazoui, J.C. Bourgoin, J. Appl. Phys. 73 (11) (1993) 7229.
[15] R.J. Walters, M.A. Xapsos, H.L. Cotal, S.R. Messenger, G.P. Summers, P.R. Sharps, M.L. Timmons, Solid-State Electronics 42 (1998) 1747.